ISSN 0021-3640, JETP Letters, 2020, Vol. 111, No. 10, pp. 575–581. © Pleiades Publishing, Inc., 2020.
Russian Text © The Author(s), 2020, published in Pis'ma v Zhurnal Eksperimental'noi i Teoreticheskoi Fiziki, 2020, Vol. 111, No. 10, pp. 682–688.

CONDENSED MATTER

Probing States of a Double Acceptor in CdHgTe Heterostructures via Optical Gating

I. D. Nikolaev[a], T. A. Uaman Svetikova[a], V. V. Rumyantsev[b], M. S. Zholudev[b], D. V. Kozlov[b], S. V. Morozov[b], S. A. Dvoretsky[c], N. N. Mikhailov[c], V. I. Gavrilenko[b], and A. V. Ikonnikov[a, *]

[a] *Faculty of Physics, Moscow State University, Moscow, 119991 Russia*

[b] *Institute for Physics of Microstructures, Branch of the Federal Research Center Institute of Applied Physics, Russian Academy of Sciences, Nizhny Novgorod, 603950 Russia*

[c] *Rzhanov Institute of Semiconductor Physics, Siberian Branch, Russian Academy of Sciences, Novosibirsk, 630090 Russia*

**e-mail: antikon@physics.msu.ru*

Received April 10, 2020; revised April 16, 2020; accepted April 16, 2020

Photoconductivity spectra in a HgTe/CdHgTe double quantum well with a normal band structure have been studied. Photosensitivity bands associated with the ionization of a mercury vacancy, which is a doubly charged acceptor, have been detected in photoconductivity spectra. The transformation of photoconductivity spectra when the Fermi level moves from the edge of the valence band through the band gap to the conduction band has been revealed using the residual photoconductivity effect. It has been shown that the observed absorption bands are due to the ionization of doubly charged acceptors rather than individual different singly charged states.

DOI: 10.1134/S0021364020100124

1. INTRODUCTION

The HgCdTe (mercury cadmium telluride, MCT) semiconductor material is a basic material for detectors and focal plane arrays of a mid-infrared range [1]. One of its main advantages is the possibility of obtaining high-quality $Cd_xHg_{1-x}Te$ ternary alloys with almost any cadmium content. The width of the band gap in these alloys can vary from 1.6 eV (at $x = 1$) to zero (at $x \leq 0.16$–0.17); this property makes MCT promising for terahertz optoelectronics.

A stronger control of the band structure can be achieved using heterostructures with quantum wells instead of bulk materials. Such heterostructures with HgTe/CdHgTe quantum wells have become in the last decade of great interest because of their unique properties. The most known examples are a transition from the normal to inverted band structure with an increase in the width of the quantum well [2, 3] and the detection of the conduction via edge states topologically protected from backscattering in the quantum well with the inverted spectrum [4]. For new applications, MCT-based heterostructures are currently considered as active media for interband lasers of the range of 30–50 μm [5, 6], which is inaccessible for quantum-cascade lasers based on III–V materials because of phonon absorption [7].

One of the features inherent in CdHgTe solid solutions and heterostructures based on them is the formation of mercury vacancies even in high-quality structures. A vacancy appears because of a weak Hg–Te bond [8]. This vacancy serves as a doubly charged acceptor because a mercury ion incorporated into the HgTe crystal lattice transfers two electrons to the valence band. In addition to an increase in the number of holes in the valence band, the vacancy makes a negative contribution to the periodic potential of the crystal lattice and can strongly affect the interband recombination times [9]. The latter property is particularly important for applications. Furthermore, MCT-based materials are characterized by the absence of a technologically "simple" shallow acceptor (as, e.g., boron for silicon). For this reason, to obtain structures with the *p*-type conductivity, mercury vacancies are often produced specially, e.g., by means of annealing [10], which naturally affects the quality of structures.

Thus, the mercury vacancy is an important "feature" of MCT-based materials; consequently, the study of its energy characteristics is relevant. However, its description is much more complex compared to, e.g., a shallow hydrogen-like center. These vacancies in MCT were studied in numerous works, but they often provide different and sometimes contradictory data on the ionization energies. To illustrate this ambiguity, the following works concerning narrow-gap MCT materials can be mentioned.

Measuring the transmission in the far infrared range, the authors of [11] determined the ionization energy of the vacancy at 10–12 meV for $Cd_xHg_{1-x}Te$ with $x = 0.2$–0.4. The same energy was obtained in [12, 13], but, in contrast to [11], the ionization energy strongly depended on the cadmium content possibly because transport methods were primarily used for the analysis. The dependence on the cadmium content was also found in [14], where acceptor states with ionization energies of 12 and 19 meV for $x = 0.216$ and 0.234, respectively, were detected. Performing a very complex analysis of photoluminescence spectra with the deconvolution of spectral lines, the authors of [15] attributed the ionization energy in the range of 12–15 meV to the mercury vacancy.

Later, the mercury vacancy in MCT ternary alloys was characterized by several ionization energies. In particular, acceptor levels elevated by 14, 18, and 27 meV from the edge of the valence band in ternary alloys with $x = 0.3$–0.4 were determined from photoluminescence spectra in [16]; some of these levels were attributed to mercury vacancies. The authors of [17] discussed the possibility that the mercury vacancy at low cadmium contents ($x < 0.33$) is a deep center with a negative Hubbard energy or a so-called *negative U* center, for which the ionization energy of the second hole from an acceptor is lower than that for the first. However, the study of photoconductivity spectra of $Cd_xHg_{1-x}Te$ epitaxial films with $x = 0.19$–0.3 in [18] showed that the ionization energy of the first hole from the neutral acceptor is 10 meV, whereas the ionization energy of the second hole is 19 meV. These energies are independent of the composition.

At the same time, studies of states of the doubly charged acceptor in MCT-based heterostructures with quantum wells have just begun with works [19–21], where photoconductivity spectra [19] and photoluminescence spectra [20, 21] of such impurity states were measured in narrow gap heterostructures ($E_g <$ 80 meV) with a normal band structure. In principle, the data obtained do not contradict each other: the spectra demonstrate bands; some of them (5–16 meV and 20–35 meV) were attributed to the excitation of the mercury vacancy. Nevertheless, the relation of the observed bands to the doubly charged acceptor was established in the cited works only in calculations.

In this work, we experimentally demonstrate that subgap features observed in photoconductivity spectra in MCT-based heterostructures are due to the ionization of the doubly charged acceptor rather than the ionization of states of two different singly charged acceptors.

2. EXPERIMENTAL PROCEDURE

The structure under study was grown by molecular beam epitaxy on 400-μm-thick semi-insulating GaAs(013) substrate [22, 23]. A buffer consisting of a 30-nm-thick ZnTe layer and a 5-μm-thick CdTe relaxed layer was grown on substrate. Then, the active part of the structure was grown, including the 30-nm-thick $Cd_{0.64}Hg_{0.36}Te$ lower barrier, the 4.5-nm-thick HgTe lower quantum well, the 3-nm-thick $Cd_{0.64}Hg_{0.36}Te$ tunnel-transparent barrier, the 4.5-nm-thick HgTe upper quantum well, and the 30-nm-thick $Cd_{0.64}Hg_{0.36}Te$ upper barrier $Cd_{0.64}Hg_{0.36}Te$. A 40-nm-thick CdTe coating layer was grown above the entire structure. The structure was not doped. The presence of two quantum wells in the heterostructure is of no significance for this work. This structure was chosen to study the subgap photoconductivity because of the pronounced residual photoconductivity [24]. The step-by-step illumination of this structure by visible light made it possible to successively change the conductivity type from the *p*-type to the *n*-type, which was not observed in structures with single quantum wells. Thus, controlled illumination allows varying the position of the Fermi level in the studied sample. This technique is sometimes called optical gating.

According to the performed calculations of the band structure [25], the sample under study has a normal band structure, which is confirmed by previous magneto-optical studies (see data on sample 150217 in [26]). We note that corrected thicknesses of the quantum wells and the barrier between them were used in [26] to achieve good agreement between the observed and calculated energies of magneto-optical transitions. According to magneto-optical measurements, the width of the band gap in the structure is ~75 meV; therefore, transitions involving studied "impurity" states will be observed in the subgap spectral range.

Samples were characterized by studying their electrophysical properties. Indium contacts in the Hall geometry were deposited on the surface of the 4 × 2-mm samples. The same samples were used to measure photoconductivity spectra. The samples were placed in a light-tight insert, which completely screened them from external radiation. A blue light-emitting diode and a miniature incandescent lamp were placed near the sample to controllably illuminate it. Slowly descending the insert in a Dewar vessel with liquid helium, we measured the longitudinal and transverse resistances in the temperature range of 4.5–300 K. An external magnetic field of 0.05 T was produced by means of a resistive solenoid. The current through the sample was 1–10 μA.

Moreover, we performed two-contact measurements of the quantum Hall effect on 5 × 5-mm samples with strip ohmic contacts. The structures were placed in a helium cryostat in the center of a superconducting solenoid (maximum field 6 T). The "blue" light-emitting diode was placed near the sample.

Photoconductivity spectra were measured at $T =$ 5 K with a Bruker Vertex 70v Fourier transform spectrometer. We used a Globar source and a Mylar Multilayer beamsplitter. The samples were placed in an

Oxford Instruments Optistat CF helium-flow cryostat, which was placed in the spectrometer so that the sample was located at the focus of the radiation beam. The cryostat was equipped with polypropylene and Lavsan windows. A cold black polyethylene filter was placed in front of the sample and the blue light-emitting diode was placed near the sample. The spectral characteristics of all used optical elements and filters allowed recording spectra in the range of 4–84 meV without the introduction of any sharp features to the spectrum. The spectral resolution was ≈1 meV (8 cm^{-1}). We used the same samples that were used to study the temperature dependences of the resistance. A photoconductivity signal was taken from current contacts.

3. RESULTS AND DISCUSSION

Figure 1 shows the temperature dependences of the resistance and carrier density in the studied structure. An activation segment corresponding to the intrinsic conductivity region is seen at high temperatures $T > 180$ K. The activation energy determined from the slope of this linear segment is $E_a \approx 70$ meV; correspondingly, the thermal width of the band gap is $E_g \approx 140$ meV, which is twice as large as the value previously determined from magnetoabsorption spectra [26]. This is assumingly due to significant fluctuations of the potential: because of these fluctuations, thermally excited charge carriers have to additionally overcome a significant barrier to reach the mobility threshold. The resistance and density approach constant values with decreasing temperature. The density under dark conditions at low temperatures is $p \approx 1.1\times10^{11}$ cm^{-2}. The *hole* conduction occurs in this case.

After short-term illumination by the incandescent lamp, the resistance of the structure increases by almost an order of magnitude (lines *2* in Fig. 1). It is noteworthy that heating to $T = 100$ K and subsequent inverse cooling hardly changed the resistance, which indicates the stable effect of the residual photoconductivity. The density, as well as the mobility, cannot be measured under these conditions.

After further short-term illumination at a low temperature, the resistance of the sample *decreases* to almost the initial values. However, the *electron* conduction occurs in this case. The density in this case is $n \approx 6\times10^{10}$ cm^{-2}. Heating to 100 K and subsequent cooling slightly increase both the resistance and density, which indicates a decrease in the mobility after heating. Heating possibly results in a certain depletion of some deep traps located, e.g., on the surface. This increases the electron density, but also increases the number of scattering centers, which reduces the mobility. The mobilities for holes and electrons in these structures at low temperatures are ~2000 and 4000 $cm^2/(V\,s)$.

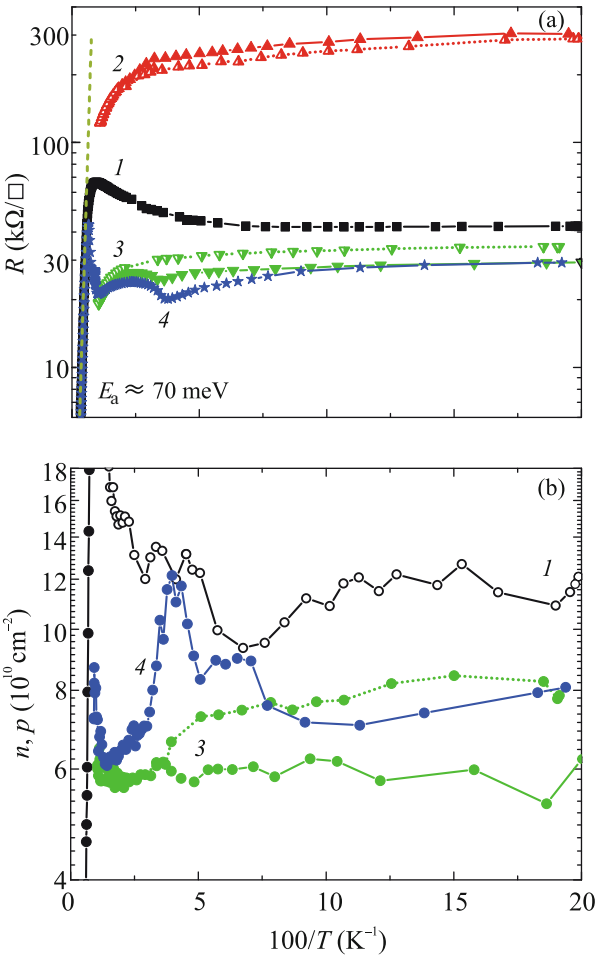

Fig. 1. (Color online) (a) Surface resistivities of the HgTe/CdHgTe double quantum well versus the inverse temperature obtained (line *1*) under dark conditions and after short-term illumination by (lines *2* and *3*) an incandescent lamp or (line *4*) a blue light-emitting diode. The solid and dotted lines *2* and *3* correspond to the heating and subsequent cooling of the sample without illumination. (b) Charge carrier density versus the inverse temperature under the same conditions. The open and closed symbols correspond to the hole and electron conductivities, respectively.

The illumination of the structure by blue light leads to the same situation as the second illumination by the incandescent lamp (lines *3* and *4* in Fig. 1). This occurs because a certain "net" density depending only on the wavelength is established upon a sufficiently long irradiation by light [24]. The wavelength of radiation of the used light-emitting diode at $T = 4.2$ K is $\lambda \approx 440$ nm, and radiation of the incandescent lamp is maximal at $\lambda \approx 1500$ nm. According to [24], long-term illumination by light with such wavelengths results in the establishment of approximately identical electron density for this structure. Thus, both the incandescent lamp and the blue light-emitting diode can be used to change the type of the conduction and

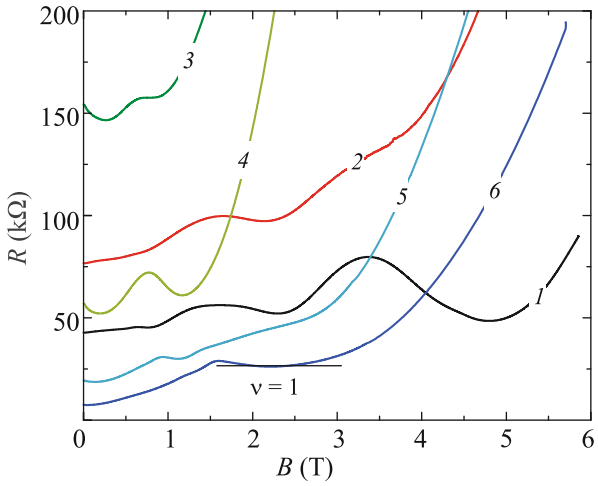

Fig. 2. (Color online) Magnetic field dependences of the resistance for the structure under study obtained (line *1*) under dark conditions and (lines *2*–*6*) after short-term illuminations by blue light. Successive illumination (lines *1*–*3*) first increases and (lines *4*–*6*) then reduces the resistance.

charge carrier density because of the effect of positive residual photoconductivity in the studied structure. However, the light-emitting diode can provide lower illumination doses and, correspondingly, allows the variation of the density with a smaller step. For this reason, we used only blue light illumination in further studies.

Figure 2 shows the dependences of the resistance of the structure measured in the two-contact scheme on the magnetic field at various doses of illumination by the blue light-emitting diode. Every line (except for dark) was recorded after switching off the light-emitting diode. It is seen that illumination first leads to an *increase* in the resistance and then, after reaching a maximum, to its *decrease*.

Figure 2 also demonstrates that the characteristic magnetic fields, at which a stepwise increase in the resistance occurs, first decrease with an increase in the illumination dose and then increase again. This stepwise increase in the resistance is due to an increase in the degree of degeneracy of Landau levels with the magnetic field. At a sufficiently high magnetic field, all charge carriers are located at a single Landau level (ultra-quantum limit). As the field is further increased, more charge carriers become localized and no longer contribute to the conductivity. This situation for a lower charge carrier density occurs at lower magnetic fields.

At high illumination doses, when the conduction occurs due to electrons, the dependences of the magnetoresistance exhibit the fundamental plateau of the quantum Hall effect. The electron density determined from the position of the plateau corresponding to the filling factor $\nu = 1$ (line *6* in Fig. 2) is 5.4×10^{10} cm^{-2}, which is in good agreement with the Hall measurements in low magnetic fields.

Landau quantization is also manifested on the dark curve (corresponding to the hole conduction), but pronounced plateaus seen for the "electron" case are not observed. This is most likely due to complex structure of Landau levels in the valence band in the HgTe quantum well [27, 28] and, particularly, in structures with double quantum wells [29, 30].

Thus, short-term dosed illuminations by blue light or light of the incandescent lamp lead to a gradual decrease in the dark hole density and to transition through an insulating state again to a conducting state but now caused by electrons. In other words, the Fermi level, initially located in the valence band, upon illumination rises in energy, passes the band gap, and, finally, enters the conduction band.

We now consider photoconductivity spectra. Figure 3 shows the photoconductivity spectra recorded immediately after the cooling of the sample (line *1*) and after successive short-term illuminations by blue light (lines *2*–*7*). All spectra exhibit an interband photoconductivity band with a cutoff at 70–75 meV. This value is in good agreement with data determined from magnetoabsorption spectra [26]. A sharp drop of the band above 80 meV is due to a decrease in the transmission of the used beamsplitter.

Subgap photoconductivity bands at 8–16 meV (band *a*) and 19–25 meV (band *b*) are of the most interest (Fig. 3). Only band *a* is observed under "dark"[1] conditions (line *1*). In this case, resistance of the sample is close to the dark resistance in Fig. 1. Short-term illumination results in the appearance of band *b* in the spectra (lines *2* and *3* in Fig. 3). In this case, the resistance of the sample *increases*. The further illumination of the sample reduces the intensity of band *a* (line *4*) and eliminates it (line *5*), whereas band *b* holds. At the same time, the resistance continues to increase, reaching a maximum of several megohms. Finally, the further dosed illumination *reduces* the resistance. In this case, both bands *a* and *b* in photoconductivity spectra disappear (lines *6* and *7*).

To explain the observed behavior of subgap features of photoconductivity spectra, we use the scheme illustrating the ionization energies of the doubly charged acceptor with respect to the bands (Fig. 4). This scheme is based on the calculation of the band structure in [26] and the calculation of the ionization energies of the bivalent acceptor in [19] (the dispersion of ionization energies depending on the position of the mercury vacancy with respect to the center of the quantum well results in a certain broadening of bands *a* and *b* of the photoconductivity). The "dou-

[1] The term "dark" is given in quotation marks because the sample is in any case illuminated by warm parts of the cryostat and the radiation of the Globar of the Fourier transform spectrometer.

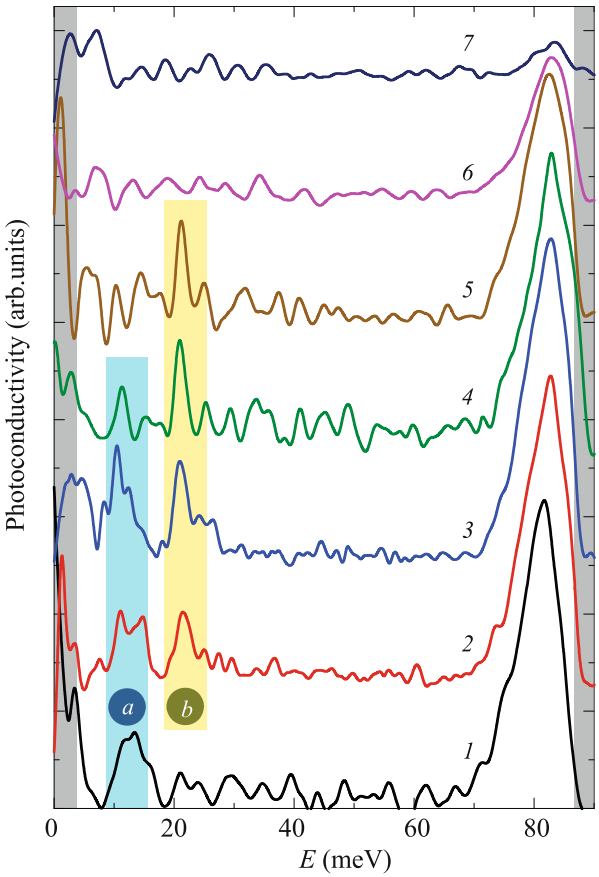

Fig. 3. (Color online) Photoconductivity spectra of the HgTe/CdHgTe double quantum well obtained (line *1*) under dark conditions and (lines *2*–*7*) after short-term illuminations by blue light. The lines are shifted in the vertical direction with respect to each other by a fixed value. Bands *a* and *b* are subgap features observed in the spectra. Gray bands at the edges of the figure are spectral regions beyond the range of a Mylar Multilayer beamsplitter.

bling" of subbands in the valence band is due to the double quantum well because the barrier between the quantum wells is much less tunnel-transparent for holes than for electrons. The energy A^0 corresponds to the single ionization of the neutral acceptor (acceptor with two holes), whereas the energy A^{-1} corresponds to the separation of the second hole from the singly ionized acceptor. The energy A^{-1} is higher A^0 because it is easier to "separate" one hole from the neutral acceptor than to separate the hole from the negatively charged singly ionized acceptor in view of the Coulomb interaction.

After cooling, the samples have the hole conduction, and the Fermi level is close to the top of the valence band (Fig. 4a). In this case, all of the mercury vacancies will be neutral. Correspondingly, photoconductivity spectra will exhibit transitions with the energy A^0 corresponding to the separation of the first hole (the transition of electrons from the valence band to the neutral acceptor). These transitions are responsible for spectral band *a* (line *1* in Fig. 3). It is noteworthy that the absence of band *b* on line *1* indicates that the energies A^0 and A^{-1} correspond to the ionization of the doubly charged acceptor rather than of two individual single-charged acceptors. In the latter case, in the situation where the Fermi level is located in the valence band, photoconductivity spectra would demonstrate both bands *a* and *b*.

After short-term illumination, the Fermi level rises and reaches the energy A^0. In this case, some neutral acceptors become singly ionized (Fig. 4b). Under these conditions, photoconductivity spectra will exhibit both bands *a* and *b* associated with the ionization of neutral and singly charged acceptors, respectively (lines *2* and *3* in Fig. 3). Owing to the dispersion of ionization energies depending on the position of the mercury vacancy with respect to the center of the

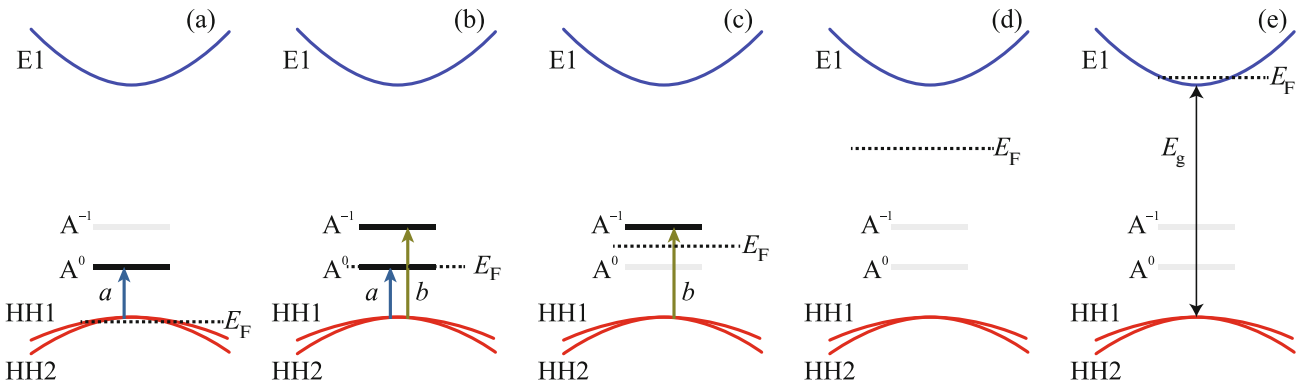

Fig. 4. (Color online) Schematic of the impurity transitions observed in photoconductivity spectra: (E1) the first size quantization subband of the conduction band, (HH1 and HH2) the subbands of the valence band, (E_F) the Fermi level, (A^0) the partial ionization energy (separation of the first hole) of the neutral mercury vacancy, and (A^{-1}) the complete ionization energy (separation of the second hole) of the singly ionized mercury vacancy. The band scheme is taken from [26]. The energies are measured from the top of the valence band. Transitions impossible at a given position of the Fermi level are given in gray.

quantum well, photoconductivity bands *a* and *b* are observed in a certain range of the Fermi level (range of illumination dose).

Further illumination increases the ionization of neutral acceptors, reducing the intensity of band *a* (line *4* in Fig. 3). Finally, when the Fermi level becomes above the energy A^0 (Fig. 4c), all acceptors will be singly ionized, and only band *b* will remain in photoconductivity spectra (line *5* in Fig. 3).

Upon the further increase in the Fermi energy, all acceptors are fully (doubly) ionized (Fig. 4d), which results in the disappearance of all subgap features of photoconductivity spectra (line *6* in Fig. 3). Finally, when the Fermi level enters the conduction band (Fig. 4e), the intrinsic electron conductivity of the sample increases, which complicates the detection of the interband photoconductivity (line *7* in Fig. 3).

The spectral positions of bands *a* (8–16 meV) and *b* (19–25 meV) are in good agreement with the data obtained for ionization energies of the mercury vacancy in various HgTe single quantum wells with the normal band structure [19–21]. Because of this agreement together with observed changes in band intensities upon variation of the position of the Fermi level, band *a* can be attributed to the ionization of the neutral mercury vacancy (separation of one hole), and band *b* can be attributed to the ionization of the singly ionized vacancy (separation of the second hole).

ACKNOWLEDGMENTS

We are grateful to L.S. Bovkun for assistance in the analysis of transport measurements.

FUNDING

This work was supported by the Russian Science Foundation (project no. 19-72-00128). The measurements of the magnetoresistance were supported by the Council of the President of the Russian Federation for State Support of Young Scientists and Leading Scientific Schools (project no. MK-1430.2020.2).

REFERENCES

1. A. Rogalski, Opto-Electron. Rev. **20**, 279 (2012).
2. L. G. Gerchikov and A. Subashiev, Phys. Status Solidi B **160**, 443 (1990).
3. B. A. Bernevig, T. L. Hughes, and S. C. Zhang, Science (Washington, DC, U. S.) **314**, 1757 (2006).
4. M. König, S. Wiedmann, C. Brüne, A. Roth, H. Buhmann, L. W. Molenkamp, X. L. Qi, and S. C. Zhang, Science (Washington, DC, U. S.) **318**, 766 (2007).
5. V. Rumyantsev, M. Fadeev, V. Aleshkin, N. Kulikov, V. Utochkin, N. Mikhailov, S. Dvoretskii, S. Pavlov, H.-W. Hübers, V. Gavrilenko, C. Sirtori, Z. F. Krasilnik, and S. Morozov, Phys. Status Solidi B **256**, 1800546 (2019).
6. G. Alymov, V. Rumyantsev, S. Morozov, V. Gavrilenko, V. Aleshkin, and D. Svintsov, ACS Photon. **7**, 98 (2020).
7. M. S. Vitiello, G. Scalari, B. Williams, and P. de Natale, Opt. Express **23**, 5167 (2015).
8. D. T. Cheung, J. Vac. Sci. Technol. A **3**, 128 (1985).
9. A. Rogalski, Rep. Prog. Phys. **68**, 2267 (2005).
10. V. S. Varavin, G. Yu. Sidorov, and Yu. G. Sidorov, Russ. J. Phys. Chem. A **84**, 1459 (2010).
11. B. Li, Y. Gui, Z. Chen, H. Ye, J. Chu, S. Wang, R. Ji, and L. He, Appl. Phys. Lett. **73**, 1538 (1998).
12. T. Sasaki, N. Oda, M. Kawano, S. Sone, T. Kanno, and M. Saga, J. Cryst. Growth **117**, 222 (1992).
13. S. H. Shin, M. Chu, A. H. B. Vanderwyck, M. Lanir, and C. C. Wang, J. Appl. Phys. **51**, 3772 (1980).
14. S. R. Kurtz, J. Bajaj, D. D. Edwall, and S. J. C. Irvine, Semicond. Sci. Technol. **8**, 941 (1993).
15. F. Yue, J. Wu, and J. Chu, Appl. Phys. Lett. **93**, 131909 (2008).
16. K. D. Mynbaev, A. V. Shilyaev, N. L. Bazhenov, A. I. Izhnin, I. I. Izhnin, N. N. Mikhailov, V. S. Varavin, and S. A. Dvoretskii, Semiconductors **49**, 367 (2015).
17. F. Gemain, I. C. Robin, and G. Feuillet, J. Appl. Phys. **114**, 213706 (2013).
18. V. V. Rumyantsev, D. V. Kozlov, S. V. Morozov, M. A. Fadeev, A. M. Kadykov, F. Teppe, V. S. Varavin, M. V. Yakushev, N. N. Mikhailov, S. A. Dvoretskii, and V. I. Gavrilenko, Semicond. Sci. Technol. **32**, 095007 (2017).
19. D. V. Kozlov, V. V. Rumyantsev, S. V. Morozov, A. M. Kadykov, M. A. Fadeev, V. S. Varavin, N. N. Mikhailov, S. A. Dvoretskii, V. I. Gavrilenko, and F. Teppe, Semiconductors **50**, 1662 (2016).
20. D. V. Kozlov, V. V. Rumyantsev, A. M. Kadykov, M. A. Fadeev, N. S. Kulikov, V. V. Utochkin, N. N. Mikhailov, S. A. Dvoretskii, V. I. Gavrilenko, H.-W. Hubers, F. Teppe, and S. V. Morozov, JETP Lett. **109**, 657 (2019).
21. D. V. Kozlov, V. V. Rumyantsev, S. V. Morozov, A. M. Kadykov, M. A. Fadeev, M. S. Zholudev, V. S. Varavin, N. N. Mikhailov, S. A. Dvoretskii, V. I. Gavrilenko, and F. Teppe, J. Exp. Theor. Phys. **127**, 1125 (2018).
22. N. N. Mikhailov, R. N. Smirnov, S. A. Dvoretsky, Y. G. Sidorov, V. A. Shvets, E. V. Spesivtsev, and S. V. Rykhlitski, Int. J. Nanotechnol. **3**, 120 (2006).
23. S. Dvoretsky, N. Mikhailov, Y. Sidorov, V. Shvets, S. Danilov, B. Wittman, and S. Ganichev, J. Electron. Mater. **39**, 918 (2010).
24. K. E. Spirin, D. M. Gaponova, K. V. Marem'yanin, V. V. Rumyantsev, V. I. Gavrilenko, N. N. Mikhailov, and S. A. Dvoretsky, Semiconductors **52**, 1586 (2018).

25. S. S. Krishtopenko, W. Knap, and F. Teppe, Sci. Rep. **6**, 30755 (2016).

26. L. S. Bovkun, S. S. Krishtopenko, A. V. Ikonnikov, V. Ya. Aleshkin, A. M. Kadykov, S. Ruffenach, C. Consejo, F. Teppe, W. Knap, M. Orlita, B. Piot, M. Potemski, N. N. Mikhailov, S. A. Dvoretskii, and V. I. Gavrilenko, Semiconductors **50**, 1532 (2016).

27. L. S. Bovkun, A. V. Ikonnikov, V. Ya. Aleshkin, K. E. Spirin, V. I. Gavrilenko, N. N. Mikhailov, S. A. Dvoretskii, F. Teppe, B. A. Piot, M. Potemski, and M. Orlita, J. Phys.: Condens. Matter **31**, 145501 (2019).

28. K. Ortner, X. C. Zhang, A. Pfeuffer-Jeschke, C. R. Becker, G. Landwehr, and L. W. Molenkamp, Phys. Rev. B **66**, 075322 (2002).

29. L. S. Bovkun, A. V. Ikonnikov, V. Ya. Aleshkin, K. V. Maremyanin, N. N. Mikhailov, S. A. Dvoretskii, S. S. Krishtopenko, F. Teppe, B. A. Piot, M. Potemski, M. Orlita, and V. I. Gavrilenko, Opto-Electron. Rev. **27**, 213 (2019).

30. M. V. Yakunin, S. S. Krishtopenko, S. M. Podgornykh, M. R. Popov, V. N. Neverov, N. N. Mikhailov, and S. A. Dvoretsky, JETP Lett. **104**, 403 (2016).

Translated by R. Tyapaev